OES25-050

Sea Experiments on Autonomous tracking of Oil Spill using a Robotic Platform

S. S. RATHOUR — Dept. of Naval Architecture and Ocean Engineering, Osaka University
E-mail: swarn@naoe.eng.osaka-u.ac.jp
Naomi KATO — Osaka University
Naoto TANABE — Osaka University
H. SENGA — Osaka University
M. YOSHIE — Port & Airport Research Institute
T. TANAKA — Port & Airport Research Institute

Abstract

The environmental impact of oil and gas leaks during the extraction, handling, and temporary storage of oil from offshore wells; or during the offshore transportation of oil via flow line, underwater pipeline, or tanker has never been more visible to the public – with the recent disaster in the Gulf of Mexico – yet the solutions currently available do not meet all the requirements in terms of performance and reliability. This research focuses on the problem of autonomous oil spill tracking in oceanic marine environments. We describe a sensor-based guidance, navigation, and control system (GNC) for oil spill tracking by autonomous surface vehicle (ASV) in unsteady and uncertain environments. First, we describe the design and development of a yacht-shaped ASV that can track spilled oil on the sea surface using data supplied by onboard sensors to control rudder angle and sail area for navigation. Secondly, we describe an autonomous ASV decision-making algorithm for target speed and direction based on a complete time history of the scanned area around the ASV by the oil detection sensor. Finally, we describe field experiments conducted at the Eigashima beach, Kobe to validate the performance of the ASV with regard to autonomous oil spill tracking using GNCS based on onboard sensors data for tracking artificial oil targets.

1. INTRODUCTION

Offshore oil spills or leaks can occur during various stages of well drilling, workover, or repair operations; during the extraction, handling, and temporary storage of oil from offshore wells; or during the offshore transportation of oil via flow line, underwater pipeline, or tanker. The physical smothering and toxic effects of spilled oil in the ocean environment can severely damage sea flora and fauna. The extent of this impact, however, depends upon the volume and the type of oil spilled, ambient conditions, and the sensitivity of the affected marine ecosystem and its inhabitants to the oil. These disasters can result in enormous damage to the ocean environment and regional economies. Moreover, in high volume, residual spilled oil washing up along the coast can cause significant long-term damage to the environment (Fingas & Charles, 2001). Due to the aforementioned reasons, oil spillage in the ocean environment requires a quick response because it can precipitate massive environmental catastrophes. Consequently, an improved method for oil spill detection and tracking is required.

The dispersion of oil in the open ocean presents a number of challenges for detection and containment. Spilled oil can spread over a wide area, depending on the meteorological and oceanography conditions, the season, and the nature of the accident. In addition, small-scale differences in the winds and currents can cause the oil slick to become patchy. Weathering of the oil slick over time makes the oil slick thinner and causes it to break apart into multiple smaller slicks of varying density as it continues to emulsify and weather. Detection of the oil spill requires advanced instruments (Fingas & Charles, 2001), especially in the case of thin oil slicks or in cases where the oil slick is not clearly visible. Presently, the primary means of spilled oil detection and surveillance on the sea surface involves the use of satellite or airborne sensors (Jensen, Andersen, Daling, Nost, 2008). Compact fluorescence lidar systems (Yamagishi, Hitomi, Yamanouchi, Yamaguchi, Shibata, 2000), using charge-coupled device (CCD) camera for imaging, are used to detect the fluorescence of substances excited by laser. This equipment can be helicopter mounted to provide images of spilled oil spreading and its classification, even in the dark. However, the remote surveillance of oceanography data via satellites and aircraft is restricted due to their temporal and geographical limitations/coverage. Helicopters, for example, cannot continuously track spilled oil because of their limited range and endurance, and the need to be mindful of the safety of the crew. Drift buoys have traditionally been used to track spilled oil (Goodman, Simecek-Beatty, Hodginse, 1999). The hull design of these drift buoys is inspired by oceanography buoys (cylindrical or spherical shapes). Comparing the performance of various oil spill-tracking buoys, Fingas (2011) reported that while Orion and Novatech buoys were quite effective in following oil slicks under test conditions, oceanographic buoys proved to be ineffective for oil spill tracking, possible as a result of having been overly susceptible to current drift. SOTAB-II,

was developed with a controllable sail to exploit ambient wind conditions for tracking the spilled oil and subjected to proof-of-concept testing at sea. By controlling the size and direction of the sail as circumstances change, SOTAB-II can drift autonomously along with the spilled oil. SOTAB-II was developed with a cylindrical body to facilitate reactions to changes in the direction of the drifting oil slick. Experimental results showed that while sail control was achieved, the drift speed of SOTAB-II was unable to match the target drifting speed (i.e., resultant speed of 3% wind speed and water current). Consequently, a yacht-shaped SOTAB-II model was proposed in order to reduce drag coefficient in water (Kato et al., 2012; Senga et al., 2013).

1.1 Concept of SOTAB-II

The mission of our tracking and predicting system is that an autonomous surface vehicle (ASV) follows the drifting oil slick automatically and sends the positioning data and hydrographic phenomena of the position to the operation base continuously. An ASV equipped with an oil detection sensor can get closer to the oil–water interface to detect oil with greater accuracy and can continuously track the spilled oil. Such a technology, coupled with satellite and other forms of data, would facilitate the coordination of recovery operations because the data collected would better inform oil-drifting simulations, thus making it possible to predict precisely where the oil spill will travel. We can watch the oil slick drifting in real-time and predict the precise destination of it using the monitoring data from the buoy. It is an advantage point that the ASV can track the oil slick during night when the air plane can't look for the sea surface and the oil. So it will avoid possibility of the loosing oil slicks (Fig.1).

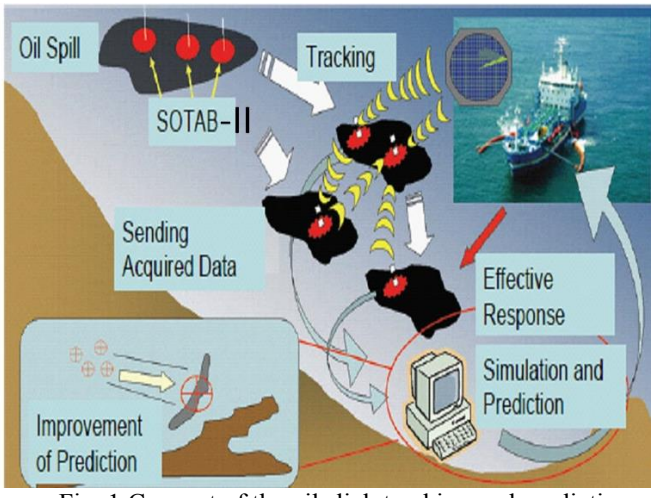

Fig. 1 Concept of the oil slick tracking and predicting system

This research addresses the problem of autonomous oil spill tracking in open waters and on the assimilation of meteorological data around the spill location to offer high-accuracy predictions of slick drifting to inform the deployment of the oil-collecting equipment along the ocean coast before oil drifts ashore. This paper describes the design of a new ASV, SOTAB-II, including embedded systems, sensor calibration and performance data, and controller and decision-making algorithms used to deduce headings and speeds based on oil sensor data is described. Finally, the results of a field experiment, using SOTAB-II fitted with a Slick Sleuth S300 as an oil detection sensor, is also described.

2. ROBOTIC PLATFOR FOR OIL SPILL TRACKING

2.1 SOTAB-II

SOTAB-II, an autonomous sailboat, is a small unmanned monohull capable of fully autonomous navigation using GPS and attitude sensor based on desired trajectory generated by its onboard GNC system. It's has been designed and developed by "Kato Laboratory" of Osaka University since 2010. It's a flexible robotic platform, capable of carrying payloads and sensors equipment's, and store those data onboard or transmit them to a land station in real time.

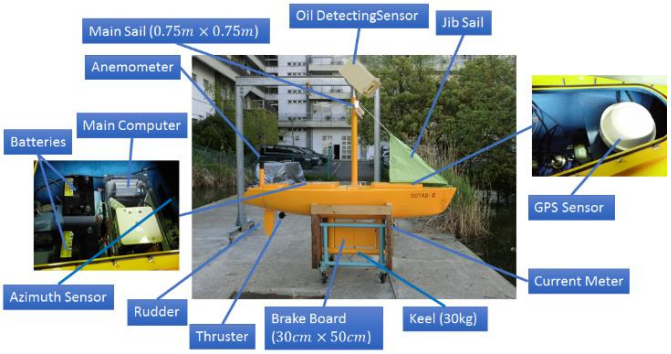

Fig. 2 SOTAB-II

The hull form of the KIT34 sailing yacht, designed by Kanazawa Institute of Technology, was chosen for the new SOTAB-II hull design (Masuyama, Nakamura, Tatano, & Takagi, 1993; see Fig. 2). Due to its wider beam and larger displacement compared to other sailing yachts of the same hull dimensions, the KIT34 hull form possesses the space requirements necessary for batteries, motors, and data acquisition and control electronics. At $^1/_4$ of the original hull size, the SOTAB-II hull is a scaled-down version of the KIT34 (Senga et al., 2013). The main hull dimensions are indicated in Table 1.

SOTAB-II is equipped with two sails, jib sail and main sail. Jib sail acts as a passive actuator trying to always keep SOTAB-II aligned with wind. The main goal of the main sail is to provide the required thrust to move SOTABII with speed specified by GNC system. The dimension of main sail was chosen as (0.75m by 0.75m), deduced from "FLUENT" (commercial hydrodynamic computational software) simulation results (Rathour et. al., 2014). For maneuvering control SOTAB-II is equipped with a single rudder system, to make sure to have sufficient steering effect in every sailing situation. Assembled inside the hull, the rudder actuators are well sealed and protected against water. In order to achieve higher stability and preventing the robot from capsizing in rough weather conditions, SOTAB-II has been augmented by a keel with a draft of .4m and mass of 30Kg for ballast bulb. Lowering the keel lowers the center of gravity of the sailboat, which makes ASV not only more stable, but also faster, as less driving power is exhausted in case of ASV remains upright. One more alteration done to original design was the addition of a brake board of flat plate to balance the aerodynamic forces acting on the upper part of the body over water surface

with the hydrodynamic forces acting on the lower part of the body below water surface. Hence a rectangular board of 0.5m in width and 0.3m in height was used.

TABLE. 1 Physical Dimensions of SOTAB-II

Total length (LOA)	2.64m
Maximum width (Beam)	0.76m
Draft	0.61m
Mast height	1.60m
Displacement	1470N
Keel position from hull bottom	0.40m
Keel weight	294N

2.2 Hardware Design

The hardware components comprising the guidance, navigation, and control system (GNCS) are located in the center of the hull. The main computer and various peripheral devices, such as serial-to-USB interfacing hardware, voltage regulator, DC to AC convertor and the wireless LAN hub, are housed in a sealed plastic fiber box. The main information-processing system for the management of data capture and autonomous control the SOTAB-II hull is an ADVANTEC ARK-1120L, a 1.66GHz device with 2GB RAM and 256GB of compact memory. Autonomous functions of the robot are facilitated by a number of sensor systems, such as GPS (A325™ GNSS smart antenna, Hemisphere GPS), ultrasonic wind anemometer (WindSonic, Gill Instruments), compass sensor (TDS01V, Vitec), water current velocity meter (AEM-RS, Japan Alcc), and oil sensor (Slick Sleuth SS300, InterOcean Systems). These sensors evaluate and inform the robot's GNCS about its location, heading, velocity, wind velocity, wind direction, water current speed, and direction. The TDS01V compass sensor is a three dimensional sensor with 3-axis accelerometer and 3-axis geomagnetic sensor onboard. The Slick Sleuth SS300 is an optical sensor that can detect micron level amounts of oil in real time from a distance of 1–5 meters above the water surface. The Slick Sleuth SS300 comes with a user-selectable detection setting, enabling the user to define the detection threshold and detection period (i.e., sampling interval/frequency), from 0.5 seconds to 90-minutes. Other than this, SOTAB-II uses five actuators for control of the sail, oil sensor, rudder, brake, and thruster (Fig. 3A).

2.3 Software Design

All software was written in Borland C++. This software manages a shared memory and thus provides communication between the individual sensor programs. For example, sensor drivers read the sensor data from the detector hardware and write it to the shared memory (Fig. 3B). Other programs requiring sensor data for processing can read data directly from the shared storage. The command signals generated by the GNCS for sail and rudder control are likewise stored in the shared memory for further analysis.

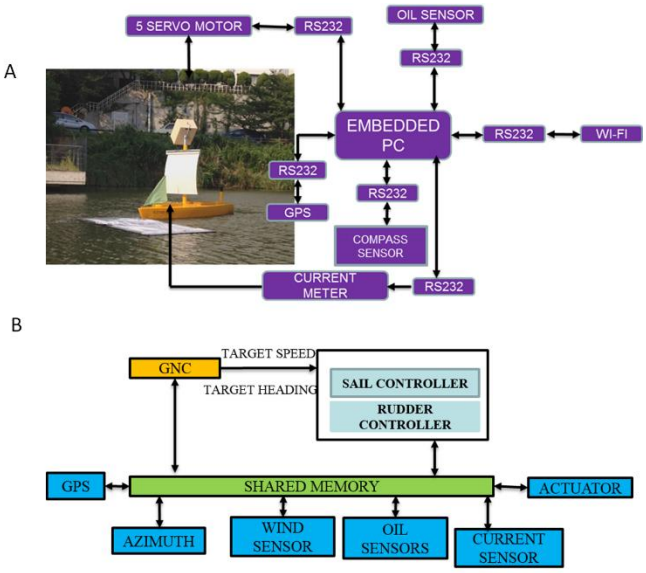

Fig. 3 (A) SOTAB-II embedded system design, (B) SOTAB-II software architecture

3. GNC SYSTEM

As described previously, SOTAB-II uses various sensors for navigation. This section describes the decision-making process for deriving the control input from the sensor information. Altogether, SOTAB-II relies on five sensors for autonomous oil spill detection and tracking. The three major control components are the main sail area, the rudder angle, and the brake board. Moreover, the oil sensor is rotated continuously in a footprint of 30 deg, to skim the area around the SOTAB-II. The heading and speed of SOTAB-II is decided after determining the robot's present position relative to the oil slick as determined based the on oil sensor data.

Some SOTAB-II data is measured by an absolute value, such as GPS data using the earth coordinate; on the other hand, some data is defined by relative values, such as the wind velocity measured by the anemometer, which only provides relative values in body coordinates. Consequently, it is necessary to coordinate between these disparate data forms by merging them into the same form. Coordinate systems are defined for the control system design by XY (i.e., earth fixed coordinate system) and $X'Y'$ (body fixed coordinate system, see Fig. 4A). Some of these parameters are obtained directly from the measuring instruments, such as $|\overrightarrow{W_r}|$(relative wind speed) and γ (wind relative heading), measured by the anemometer; $|\overrightarrow{CW_r}|$ (relative water current speed) and ζ (water current relative heading), measured by the water current meter; $|\vec{V}|$(absolute SOTAB-II drifting speed) and α (absolute SOTAB-II drifting direction), measured by GPS; and θ (angle of body coordinate relative to earth coordinate), measured by the compass sensor. On the other hand, some data, such as $|\overrightarrow{W_a}|$ (absolute wind speed), $|\overrightarrow{CW_a}|$ (absolute water current speed), β (earth coordinate-based absolute wind direction), and ξ (earth coordinate-based absolute water current direction) are calculated or deduced from the above-mentioned initially measured data. Basically, the earth fixed coordinate is set as the reference coordinate.

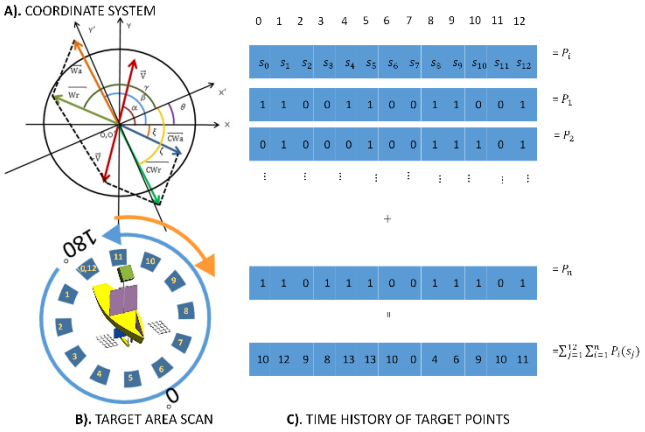

Fig. 4 (A) Coordinate System of SOTAB-II, (B) Oil Sensor Target points around SOTAB-II, and (C) Sensor data set showing time history of scanned target points.

3.1 Target Heading & Target Speed Derivation Algorithm

The oil sensor target area is a circular target around the SOTAB-II with a radius of 1.6m (Fig. 4B). This circular target area is divided into 12 sectors of 30°. Thirteen readings need to be taken around the SOTAB-II to determine whether the robot is within the spill, out of the spill, or at the border of the spill. To calculate the target heading (TD) & target speed (TV), the maximum number of detected sensor points is computed. The 13 readings for one complete rotation of the oil sensor are expressed in equations (1). P_i in equation (1) represents the data set for one rotation of the oil sensor, where "1" denotes successful oil detection and "0" denotes a failure to detect oil. At the start of the experiment, the decision algorithm initially waits for the first sensor data set P_i , after which P_i is updated every three seconds as it takes three seconds for the sensor to move to a new position and compute the target area reading (s_j, Fig. 4B & 4C). Based on the maximum number of detected sensor points (i.e., $\sum P_i(s_j)$ in each P_i) and the time history of the cumulative sum of sensor data for each of the target points expressed in euation1, (i.e.,$\sum_{j=1}^{12}\sum_{i=1}^{n} P_i(s_j)$) the following rules were derived:

$$P_i = \{s_0, s_1, s_2, \dots s_{12}\}, s_j = 1 \text{ or } 0 \ (j = 0,1,2,3,\dots 13) \quad (1)$$

1. ***Case A:*** If all 13 readings expressed in equation 1, are true and oil is detected by the oil sensor (i.e.,$\sum s_j \geq 12$), then it can be concluded that SOTAB-II lies within the oil spill. As long as SOTAB-II is within the oil spill, TD and TV will be calculated: $TD = \angle\left((2-5\%)\overrightarrow{w_a}, \overrightarrow{cw_a}\right)$ and $TV = |(2-5\%)\overrightarrow{w_a} + \overrightarrow{cw_a}|$.
2. ***Case B:*** If all 13 readings expressed in equations (1) are not true and oil is not detected by the oil sensor (i.e.,$\sum s_j = 0$), then it can be concluded that SOTAB-II lies out of the oil spill. In this case The TD is stated per equation 2:
$$TD_i = TD_{i-1} \quad (2)$$
3. ***Case C:*** If number of true sensor reading is less than 12 i.e., $\sum_{j=1}^{12} P_i(s_j)$ <12, it implies that SOTAB-II lies on the edge of the spill. Based on the relative position of SOTAB-II with respect to oil slick, various conditions can be defined. To deal with the worst situation i.e., in case SOTAB-II is found to be surrounded with multiple small patches of oil slick; target heading derivation algorithm has to be good enough to deal such conditions and provide target heading having highest probability to follow bigger patch. In such condition sensor data set (P_i) was scanned to find out total number of bigger oil slick patches surrounding SOTAB-II i.e.k. A Gaussian function (equation 3) was selected to decide the oil slick patch having highest probability, following which may end up SOTAB-II with biggest patch. The center of the each slick patch (oil slick patch) gives the Gaussian function center (c_{ik}, equation 4), and the length of the detected target point in each oil slick patch gives the spread of the Gaussian function (m_i). In equation 4 j_{ik} is the starting indices of subarray having k_i number of detected points in sensor data set. The Gaussian function data set formed using equation 3, was multiplied element wise with the cumulative sum of target points (time history of target points, i.e. $\sum_{j=1}^{12}\sum_{i=1}^{n} P_i(s_j)$; equation 5, see Fig. 5C). Total product sum of the element wise multiplication of $\sum_{j=1}^{12}\sum_{i=1}^{n} P_i(s_j)$ and Gaussian functions (equation 3) was compared to find the largest product sum (sum_{ik}). Target heading (TD) will be given by the center of the Gaussian function having largest product sum using equation 5.

$$f(g_{ijk}) = e^{-((j)-c_{ik})^2/2*{m_i}^2} \quad (3)$$

$$c_{ik} = \frac{2*j_{ik}+m_i-1}{2}, \ k = 1,2,\dots . k_i \quad (4)$$

$$sum_{ik} = \sum_{j=0}^{12}\{\sum_{j=0}^{12}\sum_{i=1}^{n} P_i(s_j)\} \times f(g_{ijk}) \quad (5)$$

$$TD = \begin{cases} c_{(i-1)k_{i-1}} & if\left(\max(sum_{(i-1)k_{i-1}}) > (\max(sum_{ik})\right) \\ c_{ik} & if(\max(sum_{ik}) > \left(\max(sum_{(i-1)k_{i-1}})\right) \end{cases} \quad (6)$$

While calculating the Gaussian functional value enough care should be taken in calculating the distance of the target point from the oil slick patch center .i.e. as the target points are defined in a circular pattern around SOTAB-II, hence clockwise and counterclockwise distance should be considered and minimum of both should be taken. As the mathematical average of the angular position of target points within the group having largest sum_{ik} will be target heading. Target heading will be given by equation 6.

3.2 Target Heading Modification based on environmental conditions

As SOTAB-II is a wind powered robot, it's highly dependent on the wind direction, because of which it cannot sail in all the directions. This limitation of SOTAB-II implies modification in the TD, based on the environmental condition. Henceforth target heading will be represented by TD and modified target heading will be represented by TD'. TD' will be determined using the following rules:-

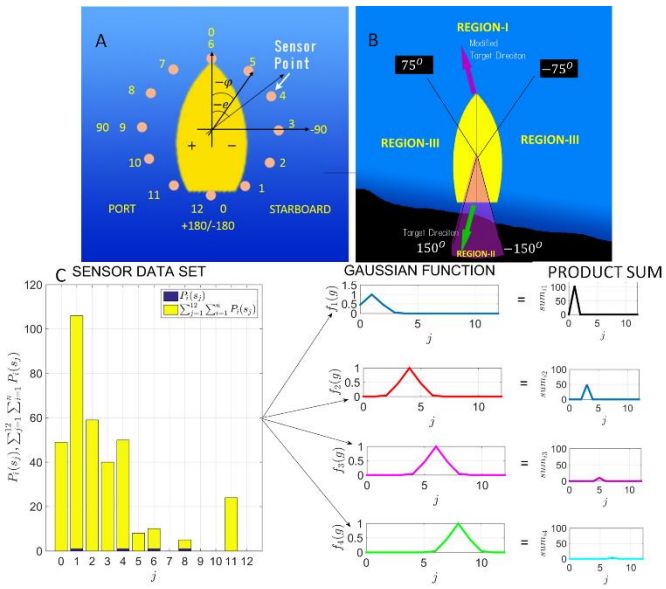

Fig. 5 (A) Oil Senor target points, (B) Modification of target heading and target speed based on the environmental condition and the region in which target heading lies, and (C) Element wise multiplication of time history of sensor data set and the Gaussian function to derive target heading.

1. **Case D*:*** - $|TD| \leq 75$ (Region I, Fig. 5B) in above mentioned range SOTAB-II is tracking the leading edge of the spill. For TD lying in region-I, TD' is given by equation. 7.

$$TD' = TD \tag{7}$$

2. **Case E*:*** - $|TD| \geq 150$ (Region II, Fig. 5B) in above mentioned range SOTAB-II is tracking the trailing edge of the spill. For TD lying in region II, TD' is given by equation. 8.

$$TD' = TD + 180 \tag{8}$$

3. **Case F & G*:*** - For TD lying in region III TD' should be decided, taking wind direction into consideration. Relative wind direction (γ), will be termed as "negative wind" if it flows from port side to starboard side and "positive wind" vice versa. For target heading lying in Region-III, wind direction relative to body fixed x-axis should be taken care of (Fig. 5B).

    a. **Case F**: -If TD and wind heading (γ), both are on the opposite side of body fixed x-axis then, TD' is given by equation. 9, (Fig. 5B).

$$TD' = \gamma \tag{9}$$

    b. **Case G**: -If TD and wind heading (γ), both are on the same side of body fixed x-axis then TD' is given by equation. 10 (Fig. 5B).

$$TD' = TD \tag{10}$$

3. 3 Target Speed Modification

The same criteria, as explained in the case of target heading, will be followed with target speed. Henceforth, target speed will be represented by TV and modified target speed will be represented by TV'. Hence, the main focus is to bring SOTAB-II inside the slick whenever it tries to go along the edge of the oil slick. Based on the assumption above, the modified target speed will be derived based on the oil sensor data.

1. **Case H**: If all 13 readings expressed in equations 1 are true (i.e., oil is detected by the oil sensor), then it can be concluded that SOTAB-II lies within the spilled oil then TV' is determined by equation 11

$$TV' = |(2 - 5\%)\overrightarrow{w_a} + \overrightarrow{cw_a}| \tag{11}$$

2. **Cases I & J**: If the target heading is in the range of $105 \leq |TD| \leq 180$, SOTAB-II speed should be reduced by 0.1% of the resultant speed of $(2 - 5\%)\overrightarrow{w_a}$ and $\overrightarrow{cw_a}$ (Case J, Eq.12***)*** and if it's in the range of $0 \leq |TD| \leq 75$, SOTAB-II modified target speed should be increased by 0.1% in resultant speed of$(2 - 5\%)\overrightarrow{w_a}$ *and* $\overrightarrow{cw_a}$ (Case I, Eq.13***)*** (Fig. 5B).

$$TV' = \max(V, TV) - 0.1\% * TV \tag{12}$$

$$TV' = \min(V, TV) + 0.1\% * TV \tag{13}$$

The max and min used in the equation above are mathematical min and max. The core idea is to move the apparatus into the slick as quickly as possible. The Slick Sleuth is a digital sensor and gives information about the presence or absence of oil. Hence, based on TD and the region in which it lies it was decided to increase or decrease TV by 0.1%. For optimal and efficient control of SOTAB-II, the continuous control signal is generated for controlling the sail area and the rudder angle based on TV' and TD'.

3.4 Sail, Rudder & Brake Board Control

Sail Control: As explained above, the drift velocity of SOTAB-II depends solely upon the main sail. The sail length is controlled via a proportional-integral-derivative controller (PID). TV', derived from the oil sensor data set, acts as a reference point for the PID controller. Moreover, SOTAB-II's drifting speed (i.e.,V) provides the feedback for the PID loop (Fig. 6A). If $V > TV'$, then the sail area is reduced, and if $V < TV'$, the sail area is increased.

Rudder Control: The maximum rudder angle is limited to $\pm 30^o$ Rudder motor control signals are generated by the PID controller where a heading error (e) is in the range of $\pm 20^o$; if out of this, a rudder range control signal of $\pm 30^o$ is generated based on the e sign (Fig. 5A). Therefore, e will be negative if SOTAB-II needs to turn starboard, and e will be positive if it needs to turn port. TD' can be in the range of $-150^o < TD' < 150^o$ (i.e., Region I or Region II).

However, this design is not good since higher TD' values may lead to rudder saturation and integral windup. To avoid this problem, TD' is scaled down by a factor g in the PID control law. Therefore, the heading error can be defined as shown in equation 14. In order to anchor the robot's position to the oil slick within the maneuverable range of the rudder, a heading error input to rudder PID control law (Fig. 6B) for tracking of a time-varying target heading was designed according to equation 15.

$$e = g * TD' - \theta \tag{14}$$

$$\delta(t) = e(t) + Kde(\dot{t}) + K_i \int e(\tau)d\tau \tag{15}$$

Broadly speaking, the relative position of SOTAB-II with respect to the slick can be divided into three states: edge mode (i.e., Case C & D,$\sum s_j < 12$), in mode or surrounded by oil (i.e., Case A, $\sum s_j \geq 12$), and out of slick (i.e.$\sum s_j = 0$). Consequently, SOTAB-II autonomously maneuvers itself to move inside the slick if $\sum s_j < 12$, by not varying TD' in equation 15 during edge or out modes unless it has achieved the required maneuver.

Brake Board Control: In the case of the brake board, only two positions are selectable: "off" and "on. "Off" denotes the condition for decreasing the drag force where the face of the brake board with the maximum surface area is oriented along the longitudinal direction of the SOTAB-II. "On" denotes the condition for increasing the drag force where the face of the brake board is perpendicular to the longitudinal direction of the SOTAB-II. Respective brake board orientation is determined based on the dynamic responses of SOTAB-II; namely, the brake board is positioned "off" in case the wind force is not capable of providing enough thrust for SOTAB-II to catch the oil slick or if it loses track of the oil slick and has to look for it again.

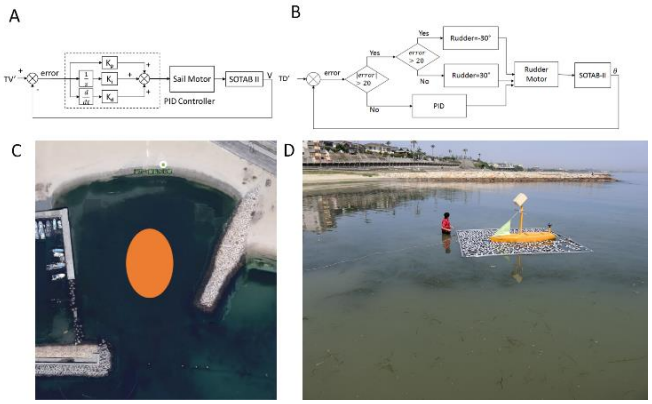

Fig. 6 (A) Main sail PID controller, (B) Rudder Controller, (C) Experimental site and (D) Floating fence to restrict the initial drift of SOTAB-II & Neoprene sheet

4. EXPERIMENTAL RESULTS

Various attempts were made to verify and optimize the control scheme. Field experiments were performed in the Eigashima beach, Kobe Japan (Fig. 6C). The field experiments were conducted to validate SOTAB-II's autonomous oil spill tracking capabilities and to test the guidance and navigation capability of SOTAB-II based on input from onboard sensors and control logic to derive target headings and directions. Neoprene sponge rubber, of diameter $0.10\ m$ and a thickness of 10mm, was used to simulate an oil spill in this experiment (Matsuzaki & Fujita, 2013). Before the start of the experiment, a floating fence $(4 * 4m^2)$ was used to restrict the initial drift of the neoprene sponge rubber and SOTAB-II (Fig. 6D). However, the neoprene sponge rubber was found to scatter and rapidly drift outside the detection zone of the oil sensor. Therefore, the control system was evaluated while the oil sensor could still detect them.

Figure 7 shows the time history of m (length of largest subarray i.e. oil slick patches surrounding SOTAB-II), k (total number of largest subarray), and $\sum_{j=1}^{12} P_i(s_j)$ (sum of detected points in sensor data set at each time instant). We can see that at $t = 313\ s, \sum P_i = 4, k = 4, m_i = 1$, this implies that there are four cluster of detected point each of length one. The starting indices of all the sequences have been shown in Fig.8. From Fig. 8 we can see that the staring indices of all the four sequence of the largest subarray at $t = 313\ s$, was found to be 1, 4, 6 and 8. Hence based on the Gaussian based product sum algorithm, four Gaussian function with center 1, 4, 6 and 8; and spread of 1was defined. The probability of each target point belonging to the four group of oil slick patch was decided based on equation 5. Figure. 9 shows the time history of product sum of each oil slick patch encountered while tracking oil slick. From Fig. 9 we can confirm that slick patch 1was found to have largest product sum among all the four slick patch, which implies that target heading will be the center of oil slick patch 1 i.e. $TD = -150^o$. Same was reflected in the time history of TD (Fig. 9).

Figure. 10 shows the time history of target heading (TD), modified target heading (TD') and relative wind direction (γ) at each instant of time. TD is calculated based on equation. 8. As explained above that at every time instant product sum of the Gaussian function data set and the time history of cumulative sum of sensor data set, i.e. $\max(sum_{ik})$ is compared with the previous product sum i.e. $\max(sum_{(i-1)k})$ and TD is decided based on the oil slick patch having largest product sum value. This was done because there will be higher probability for the buoy to find neoprene sheet if it goes in the direction of the oil slick patch having largest product sum value. Same was shown in the time history of TD (Fig. 10). From Fig. 9 we can see that cluster having largest sum was found around time $t = 313s$, at the same time instant $TD = -105^o$. Due to which after that TD was always taken as -105^o. Figure 11 shows relative position of SOTAB-II with respect to the neoprene sheet at different time instant during the experiment. SOTAB-II was found to track neoprene sheet effectively while drifting with the slick.

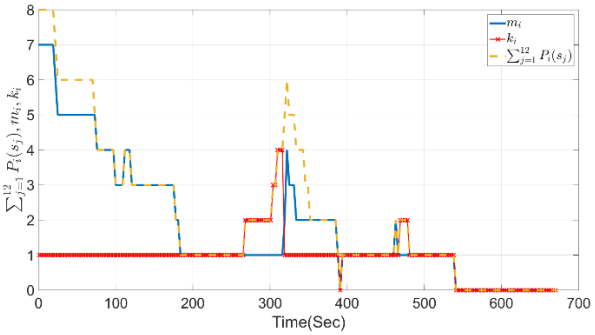

Fig.7 Total number of target points detected in each scan, length of largest subarray, total number of largest subarray in each sensor data set

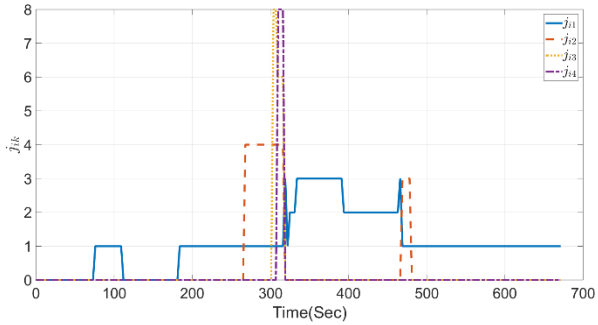

Fig.8 Time history of starting indices of each biggest cluster of detected points in sensor data set.

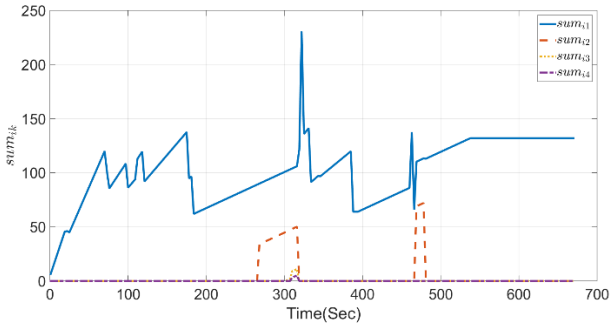

Fig.9 Time history of Sum of each cluster obtained after element wise multiplication of time history of cumulative sum of sensor data set and the Gaussian function.

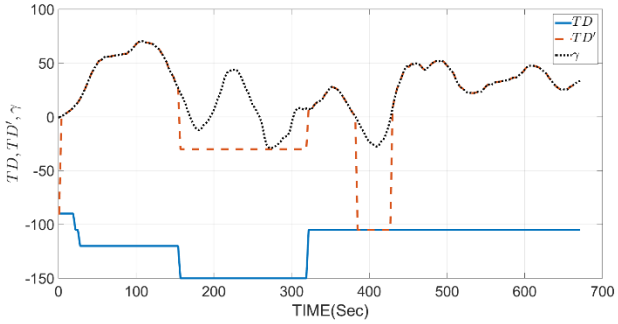

Fig. 10 Time history of variation $TD, TD' \& \gamma$ at every time instant

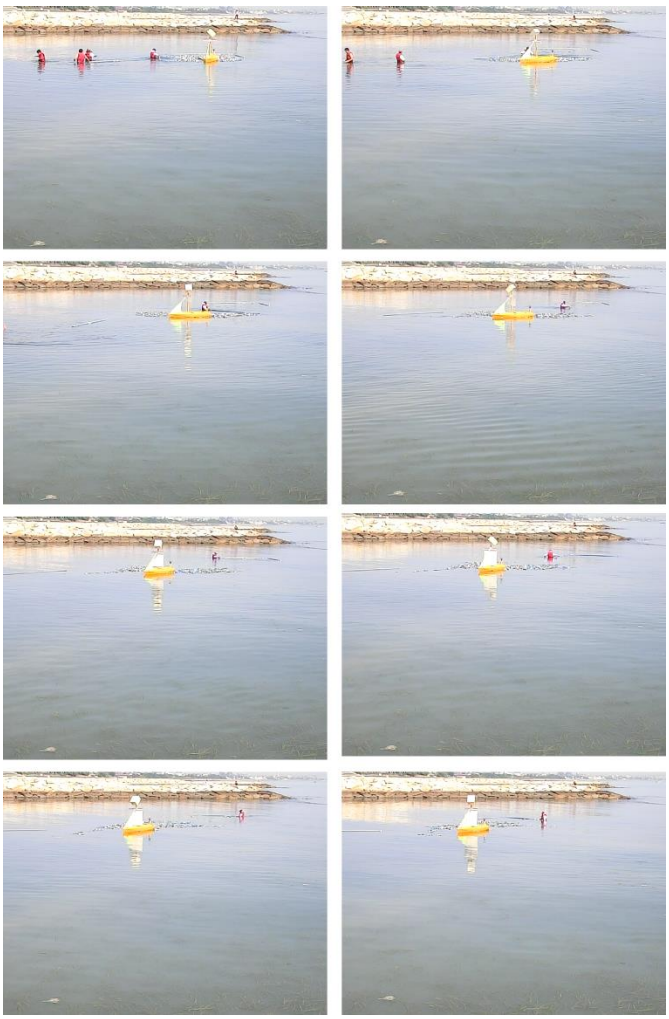

Fig.11 SOTAB-II relative position with respect to the neoprene sheet at different time instant

5. CONCLUSION

In order to overcome the limitations of existing oil spill monitoring methods, SOTAB-II, equipped with a sail (the orientation and size of which are adjustable) and sensors to detect oil slicks on the sea surface was developed. This paper described the GNCS for SOTAB-II, including real-time decision-making, to autonomous track spilled oil in unsteady and uncertain environments. The sensor-based GNCS was validated through field experiments at the Eigashima beach, Kobe Japan; the results of which illustrate the ability of SOTAB-II to autonomously track neoprene sheets, as an artificial oil slick, using an oil detection sensor. These experiments have demonstrated that SOTAB-II is capable of tracking artificial oil slick, and that the sail and rudder are effective in controlling the speed of SOTAB-II within the desired range and controlling the heading direction within the desired limits.

REFERENCES

1) Fingas, M., “Buoys and devices for oil spill tracking,” In International Oil Spill Conference. p. abs9. Washington, DC: International Oil Spill Conference Proceedings. doi:10.7901/2169-3358-2011-1-9, 2011.

2) Fingas, M., & Charles, J., “The basics of oil spill cleanup,” (2nd ed.). Boca Raton, FL: Lewis Publishers. 256 pp., 2001.

3) Goodman, R., Simecek-Beatty, D., & Hodgins, D., “Tracking buoys for oil spills,” In International Oil Spill Conference. pp. 3–8. Washington, DC: International Oil Spill Conference. doi:10.7901/2169-3358-1995-1-3, 1995

4) Jensen, H., Andersen, J., Daling, P., & Nøst, E., “Recent experience from multiple remote sensing and monitoring to improve oil spill response operations,” In International Oil Spill Conference. pp. 407–412. Washington, DC: International Oil Spill Conference Proceedings. doi:10.7901/2169-3358-2008-1-407, 2008.

5) Kato, N., Senga, H., Suzuki, H., Okano, Y., Ban, T., & Takagi, Y., “Autonomous spilled oil and gas tracking buoy system and application to marine disaster prevention system,” In Interspill Conference. London, UK: Interspill, 2012.

6) Masuyama, Y., Nakamura, I., Tatano, H., & Takagi, K., “Dynamic performance of sailing cruiser by full-scale sea tests,” In 11th Chesapeake Sailing Yacht Symposium. pp. 161–179. Jersey City, NJ: Society of Naval Architects and Marine Engineers, 1993.

7) Matsuzaki, Y., & Fujita, I. , “Horizontal turbulent diffusion at sea surface,” Journal of Society of Civil Engineering & Coastal Engineering, 69(2). pp. 460-480, 2013.

8) Rathour, S. S., Akamatsu, T., Kato, N., Senga, H., Tanabae, N., Yoshie, M. et al., “Modelling and control design of spilled oil tracking autonomous buoy,” In 24th International Ocean and Polar Engineering Conference. pp. 632-640. Busan, Korea: International Society of Ocean and Polar Engineers, 2014.

9) Senga, H., Kato, N., Suzuki, H., Akamatsu, T., Yu, L., Yoshie, M., & Tanaka, T., “Field experiments and new design of a spilled oil tracking autonomous buoy,” Journal of Marine Science and Technology. 19(1):90–102. doi:0.1007/s00773-013-0233-2, 2013.

10) Yamagishi, S., Hitomi, K., Yamanouchi, H., Yamaguchi, Y., & Shibata, T., “Development and test of a compact lidar for detection of oil spills in water,” In Second International Asia-Pacific Symposium on Remote Sensing of the Atmosphere, Environment, and Space. pp. 136–144. Sendai, Japan, 2000.